

ANALYTIC DEVELOPMENT OF AN IMPROVED
SUPERSONIC CRUISE AIRCRAFT BASED ON
WIND TUNNEL DATA*

R. L. Roensch and G. S. Page
Douglas Aircraft Company
McDonnell Douglas Corporation

SUMMARY

Data obtained from the MDC/NASA cooperative wind tunnel program were used to develop empirical corrections to theory. These methods were then used to develop a 2.2M Supersonic Cruise Aircraft Configuration with a cruise trimmed maximum L/D of 10.2. The empirical corrections to the theory are reviewed, and the configuration alternatives examined in the development of the configuration are presented. The benefits of designing for optimum trimmed performance, including the effects of the nacelles, are discussed.

INTRODUCTION

A cooperative MDC/NASA wind tunnel test program for an MDC designed supersonic cruise aircraft configuration was conducted in 1975. Testing was conducted in the NASA Ames Research Center 9- by 7-foot supersonic wind tunnel at Mach numbers from 1.6 to 2.4, and in the Ames 11- by 11-foot transonic wind tunnel at Mach numbers from 0.5 to 1.3. A complete description of the test is presented in reference 1.

The configuration for the MDC/NASA tests was the McDonnell Douglas D3230-2.2-5E advanced supersonic transport configuration shown in figures 1(a) and 1(b). The configuration employs a modified arrow wing with 71-degrees leading-edge sweep inboard and 57 degrees leading-edge sweep outboard. The design cruise point is 2.2M.

SUMMARY OF PREVIOUS WIND TUNNEL TEST

The data from the 9- by 7-foot tunnel, shown in figures 2, 3, and 4, were presented at the 1976 SCAR Conference (reference 2). The estimates shown were based on Woodward lifting surface theory (reference 3), combined with wave drag from a supersonic area rule theory (reference 4), and skin friction drag estimates. Excellent agreement is shown between the estimated and experimental minimum drag in figure 2 for all Mach numbers. The estimated and experimental drag polar shapes differ, causing the wing body drag-due-to-lift to be overpredicted below 2.0M, underpredicted above 2.0M and to agree at 2.0M. Agreement in lift curve slopes, as shown in figure 3, is

*This work was performed under NASA Contract NAS1-14621

excellent at the lower Mach numbers, but the agreement decreases at the higher Mach numbers. The estimated and experimental pitching moments shown in figure 4 agree well considering the difficulty of predicting pitching moments for cambered, three-dimensional configurations. This characteristic of Woodward-calculated pitching moments is observed for other slender configurations.

The results of the MDC/NASA test justified the basic design and analysis of the MDC supersonic transport configuration. Although some discrepancy exists in the drag-due-to-lift, the overall data agreement was excellent and the test served as a good base for the methods and configuration development detailed in this paper.

DEVELOPMENT OF IMPROVED ANALYSIS METHODS

DRAG-DUE-TO-LIFT

When compared to the wind tunnel data, the basic Woodward theory underpredicts the drag-due-to-lift at Mach numbers greater than 2.0 as seen in figure 2. The comparison of data to theory also shows that the theory does not accurately predict the lift-curve slope at Mach numbers greater than 2.0 as seen in figure 3. The discrepancy in lift curve slope is also seen to increase with increasing Mach number. A correction to the Woodward-theory drag was developed based on the error in predicted lift curve slope and assuming no leading-edge suction. From the discrepancy in estimated and experimental lift curve slopes, a difference in angle-of-attack at constant C_L can be calculated. The change in angle-of-attack, $\Delta\alpha$, is calculated by equation 1.

$$\Delta\alpha = C_L \left(\frac{1}{C_{L\alpha \text{ EXP.}}} - \frac{1}{C_{L\alpha \text{ THEORY}}} \right) \quad (1)$$

The supersonic flat plate (no leading-edge suction) drag term based on the angle shift, from equation 2, is then applied to the Woodward drag estimates as shown in figure 5.

$$\Delta C_D = C_L^2 \left(\frac{\Delta\alpha}{C_L} \right) \quad (2)$$

Analysis of three additional wing planforms for which experimental data were available (references 5 and 6) showed similar trends in lift-curve-slope and drag estimates. A generalized correction factor, $\Delta\alpha/C_L$ (equation (1)), was determined and the results are shown in figure 6. The correction term is a function of the Mach number normal to a nominal leading-edge sweep, Λ_{ED} , which was chosen to represent a multi-segment leading edge by a single leading-edge sweep value. This correction to the Woodward drag estimates, the transonic leading edge (TLE) correction, shows excellent agreement with the experimental data as shown in figure 7.

NACELLE-WING INTEGRATION

The Woodward program did not accurately predict the changes in drag-due-to-lift and pitching moment due to nacelle addition. The problem was in the inability of the Woodward program to model the flow diverter (pylon) and the interaction between the nacelle-shock and the wing-boundary-layer. As a result, the Woodward program did not accurately predict the nacelle-on-wing interference pressures. The measured nacelle-on-wing interference pressures are illustrated in figure 8. To correct the Woodward analysis, the program was modified to allow the inclusion of the experimental interference pressures on the wing. The ability of the program to predict pitching moments and induced drag was significantly improved, as seen in figures 9 and 10.

DEVELOPMENT OF AN IMPROVED PERFORMANCE WING

WING PLANFORM STUDY

A wing planform study was conducted using the improved methods developed above. The analysis of candidate planforms was conducted under the following constraints:

- (1) Constant Wing Area
- (2) Constant Aspect Ratio
- (3) Constant Tip Chord
- (4) Constant t/c Distribution
- (5) Constant Design C_L
- (6) Nacelle Induced Drag Not Included
- (7) 0 degree trailing-edge sweep inboard of 31% semi-span

The wing camber surface was designed using the Woodward program optimization of an isolated wing. The wing was then integrated to the fuselage by modifying the root airfoil incidence. A four degree root incidence was used for all cases. The wing-body combination was analyzed for lifting effects using the Woodward program and incorporating the TLE correction derived above. Each configuration was optimized for minimum zero-lift-wave-drag using the Arbitrary Body program (reference 4). The configurations were trimmed at the c.g. location for maximum trimmed L/D.

The planform study included variations in geometric planform and wing camber. The geometry of the planforms is shown in table 1. Although wings W38 and W40 had good L/D's, as seen in table 2, they were dropped from the analysis because of excessive wing length which resulted in the wing overlapping the horizontal tail. Wings W36 and W37 were not retained for the full analysis due to their low L/D values. The data in table 2 presents the L/D values for several steps in the analysis process to show the trades for various wings. The gross wing L/D value is obtained from the wing-alone induced drag data, as produced by the optimized wing camber. A representative lift-independent drag, as previously estimated for the baseline aircraft, is added to adjust the data to the proper L/D range for correlation with the complete aircraft performance data. The wing-body induced drag data include the effects of rotating the wing-root incidence to four degrees and adding the fuselage. The representative lift-independent drag used above is retained. The wing-

body, trimmed L/D incorporates the effect of trim drag on the wing-body data with the c.g. located to achieve the maximum L/D, while maintaining the reference lift-independent drag. At the optimum c.g. location, the tail load is up, so the trimmed L/D is greater than the wing-body L/D (C_{D_0} of the tail is included in the reference lift-independent drag). The complete aircraft L/D corrects the wing-body trimmed L/D for the differences in the skin friction and zero lift wave drag of the actual aircraft configuration.

The planform study, using the complete configuration, showed a relation of both drag-due-to-lift and configuration wave-drag-due-to-volume to the wing trailing-edge-sweep (notch ratio), with the wave drag bounding the optimization process. When the trailing edge sweep angle approaches the Mach angle, the wing area distribution, calculated by the Mach cutting planes, experiences rapid changes in cross-sectional area. As a result, the configuration wave drag-due-to-volume increases at high trailing-edge sweep angles, canceling the drag-due-to-lift benefits associated with high trailing-edge sweeps (or large notch ratios). This produces an "optimum" trailing-edge sweep at approximately one-half of the Mach cone angle as seen in figure 11. This effect made the high trailing edge sweep of wing W33 and W39 less beneficial than the gross wing data of table 2 indicated, showing the importance of analyzing the complete aircraft when selecting the optimum wing planform.

The four most promising wings from the planform study are shown in figure 12. Based on the cruise L/D and consideration of structural weight, trailing edge flaps, and aileron effectiveness, wing W35 was chosen for further analysis.

WING ASPECT RATIO STUDY

An aspect ratio study was conducted based on the wing W35 planform. Three alternate methods for varying the aspect ratio were investigated. They were: (1) constant trailing-edge sweep or notch ratio (inboard panel L.E. sweep is allowed to vary); (2) constant leading-edge sweep (T.E. sweep is allowed to vary); (3) constant leading- and trailing-edge sweeps (tip chord is allowed to vary). The geometry of the study wings is given in table 3. The resultant L/D's for each approach, summarized in figure 13, are presented below for each type of planform constraint.

(1) Trailing-Edge Sweep Constant: As trailing-edge sweep was the key parameter for drag as shown in figure 11, an aspect ratio study was conducted at constant trailing-edge sweep.

<u>AR</u>	<u>L/D_{TRIMMED}</u>	<u>COMMENTS</u>
1.70	9.25	increased induced drag
1.84	9.60	base case
2.08	9.05	wave drag and induced drag penalty due to decreased L.E. sweep.

(2) Leading-Edge Sweep Constant: To evaluate the penalty shown for the high aspect ratio wing with fixed trailing-edge sweep, the analysis was repeated for constant leading-edge sweep:

<u>AR</u>	<u>L/D</u> <u>TRIMMED</u>	<u>COMMENTS</u>
1.84	9.60	base case
2.08	9.66	40 degrees trailing edge sweep may cause degraded flap and aileron authority, additional low speed analysis required

(3) Leading-Edge Sweep Constant and Trailing-Edge Sweep Constant: Due to the strong impact of both leading- and trailing-edge sweeps in the previous analysis, a case was run holding all sweeps constant:

<u>AR</u>	<u>L/D</u> <u>TRIMMED</u>	<u>COMMENTS</u>
1.61	9.27	increased induced drag
1.84	9.60	base case
2.09	9.47	wave drag penalty due to wing volume and induced drag penalty due to short tip chords.

The base case aspect ratio was near the optimum in all three studies, so the base aspect ratio of 1.84 was retained for the subsequent analyses.

WING-NACELLE INTEGRATION STUDY

The classical approach to nacelle integration (reference 7) for supersonic aircraft is to reflex the wing trailing edge in the region of influence of the nacelle interference pressures as shown in figure 14. The reflex is designed to cancel the change in wing loading generated by the nacelle-on-wing interference pressure. This approach attempted to eliminate the change in drag-due-to-lift produced by the nacelle interference, but did not fully consider that there may be a benefit in the trimmed configuration performance due to the change in pitching moment produced by the nacelle installation. Results of the 1975 MDC/NASA wind tunnel test (ref. 1) showed the reflex tested did not produce a favorable nacelle interference for the trimmed aircraft configuration. The loss in pitching moment with the nacelles installed created a significant loss in trimmed L/D for the design c.g. location. An improved wing-nacelle integration procedure was developed which includes the effect of the nacelle installation on the configuration pitching moment in addition to the effect on drag-due-to-lift.

The current procedure for wing-nacelle integration is based on the selection of the wing camber which will produce the maximum trimmed L/D for a specified c.g. location. The relation of maximum trimmed L/D to wing camber (referenced by the zero-lift pitching moment coefficient) and c.g. location is shown in figure 15. In figure 15, the maximum trimmed L/D attainable for a given c.g. location is shown by the envelope curve created from the plots of trimmed L/D as a function of c.g. location for the individual pitch-constrained wings. Each point on the envelope is a specific pitch-constrained wing. Therefore,

for any design c.g. location a wing can be defined which produces the maximum trimmed L/D.

The effect of nacelle addition on a fixed geometry wing is shown in figure 16. It is seen that if the design c.g. location is near the c.g. location for maximum trimmed L/D for a specified wing geometry, a favorable nacelle interference is obtained. If the design c.g. is sufficiently forward of the optimum c.g. location, a nacelle installation penalty may occur.

For cases where the design c.g. is forward of the optimum c.g. for the L/D envelope, shown in figure 15, a local wing reflex can be added which will result in a trimmed L/D greater than that for the non-reflexed wing. As seen in figure 17, a greater amount of reflex is desired as the c.g. location is moved farther forward. The reflexes shown on figure 17 are simple geometric reflexes (see inset, figure 14) that cancel approximately 50 percent and 100 percent of the nacelle induced wing loading.

The combination of re-camber and/or reflex results in the maximum L/D envelopes shown in figure 18. The amount of reflex used for the reflexed wing envelope increases as the c.g. moves forward until 100 percent alleviation of the nacelle induced load is achieved. Note that if the design c.g. location is not constrained to be forward of the c.g. location for maximum L/D of the re-cambered wing envelope, then there is no increase in L/D available for a reflexed and re-cambered wing. Since fuel pumping can be used for c.g. control, the re-cambered wing without reflex was selected for the aircraft. The resultant c.g. location at 37 percent MAC is equivalent to zero static margin for the rigid wing.

HORIZONTAL TAIL OPTIMIZATION

Since the MDC AST configuration uses a tail upload for trim to obtain a favorable trim drag, it is appropriate to consider optimizing the horizontal tail for its trim loading. The horizontal tail used in the 1975 MDC/NASA test was flat (no camber or twist) with a biconvex airfoil section and, as such, was not optimized for minimum drag-due-to-lift at its trim C_L . The experimental tail-on data are shown in figure 19. The experimental tail drag polars (with coefficients based on wing area) for three airplane angles of attack are shown in figure 20. (The estimated polar was calculated for the uncambered tail without the wing induced flowfield.) As shown, the estimated and experimental polar shapes are in good agreement. The C_L for minimum drag, C_{L_0} , shows a shift in the experimental polar relative to the estimate. The shift in C_{L_0} is due to the presence of a wing-induced flowfield which created an adverse, non-uniform onset flow at the tail. The resulting negative C_{L_0} of the experimental data has an adverse effect on trimmed L/D.

The L/D potential for an optimum tail was assessed by analysis of a series of tails with varied C_{L_0} values in a linear trim drag program. An approximation of the camber drag expected for the tail was included. The analysis showed a 0.2 improvement in trimmed L/D for the optimum tail, as shown in figure 21. An optimum tail has not been designed due to the inability of the Woodward program to adequately analyze a tail in the presence of the wing flowfield.

CONCLUSION

Results of the design studies described above, summarized in figure 22, have been used to develop a refined AST configuration with an estimated L/D of 10.18. The changes incorporated in the refined configuration are illustrated in figure 23, along with the 1975 MDC/NASA test configuration. The refined configuration is designated as the model D3232-2.2-3 and is shown in figure 24.

A cooperative MDC/NASA wind tunnel test is currently being planned to verify the performance estimated for the refined configuration described above. The existing model fuselage and tails will be retained, so the effects of fuselage shaping and the optimum tail design will not be verified. The primary objectives of the test are:

- o Verify TLE correction
- o Confirm performance improvements for W35
- o Validate new nacelle installation procedure
- o Obtain expanded nacelle-on-wing interference pressure data base for use in developing analytical prediction methods
- o Obtain expanded horizontal tail drag data base to validate future wing-body-tail analysis and design methods

The test is expected to be conducted in a NASA facility in 1980.

SYMBOLS AND ABBREVIATIONS

α	angle of attack
$\frac{\Delta\alpha}{C_L}$	correlation factor for the TLE correction
η	span fraction
Λ	sweep angle
Λ_{ED}	equivalent derived sweep angle
Λ_{LE}	leading edge sweep angle
Λ_{TE}	trailing edge sweep angle
ϕ	angular change in slope of the wing camber surface
AR	wing aspect ratio
AST	Advanced Supersonic Transport
C_D	drag coefficient
C_{D_0}	lift independent drag coefficient
C_L	lift coefficient
$C_{L\alpha}$	lift curve slope
C_{L_0}	lift coefficient for minimum drag
C_m	pitching moment coefficient

C_{m_0}	zero lift pitching moment coefficient
c.g.	center of gravity
$\frac{dz}{dx}$	wing camber surface slope in the freestream direction
i_H	horizontal tail incidence
L.E.	leading-edge
L/D	lift to drag ratio
M	Mach number
M_0	freestream Mach number
MAC	mean aerodynamic chord
MDC	McDonnell Douglas Corporation
t/c	thickness to chord ratio
T.E.	trailing-edge
TLE	transonic leading edge

REFERENCES

1. R. L. Radkey, H. R. Welge, and J. E. Felix: Aerodynamic Characteristics of a Mach 2.2 Advanced Supersonic Cruise Aircraft Configuration at Mach Numbers From 0.5 to 2.4. NASA CR-145094, 1977.
2. R. L. Roensch: Aerodynamic Validation of a SCAR Design. Proceedings of the SCAR Conference - Part 2, NASA CP-001, [1977], pp. 155-168.
3. F. A. Woodward, E. N. Tinoco, and J. W. Larsen: Analysis and Design of Supersonic Wing-Body Combinations, Including Flow Properties in the Near Field. Part I - Theory and Application. NASA CR-73106, 1967.
4. A. E. Gentry, D. N. Smyth, and W. R. Oliver: The Mark IV Supersonic-Hypersonic Arbitrary Body Program. AFFDL-TR-73-159, 1973.
5. O. A. Morris, D. E. Fuller, and C. B. Watson: Aerodynamic Characteristics of a Fixed Arrow-Wing Supersonic Cruise Aircraft at Mach Numbers of 2.30, 2.70, and 2.95. NASA TM-78706, 1978.
6. R. B. Savelle III, and E. J. Landrum: Theoretical and Experimental Study of Twisted and Cambered Delta Wings Designed for a Mach Number of 3.5. NASA TN D-8247, 1976.
7. R. J. Mack: A Numerical Method for Evaluation and Utilization of Supersonic Nacelle-Wing Interference. NASA TN D-5057, 1969.
8. E. Bonner, M. H. Roe, R. M. Tyson, and R. Y. Mairs: Influence of Propulsion System Size, Shape, and Location on Supersonic Aircraft Design. NASA CR-132544, 1974.

TABLE 1.- WING PLANFORM GEOMETRY SUMMARY

PLANFORM REFERENCE NUMBER	LEADING EDGE			TRAILING EDGE	
	Δ INBOARD (DEGREES)	y BREAK (% SEMISPAN)	Δ OUTBOARD (DEGREES)	y BREAK (% SEMISPAN)	Δ OUTBOARD (DEGREES)
W33	71	NONE	N/A	30	46
W34*	71	63.6	57	30	17
W35	71	70	61.5	30	31
W36	61	NONE	N/A	NONE	0
W37	65	NONE	N/A	30	18
W38	74	NONE	N/A	30	62
W39	74	70	62	30	43
W40	74	55	62	30	25

*BASELINE

TABLE 2.- WING PLANFORM PERFORMANCE SUMMARY

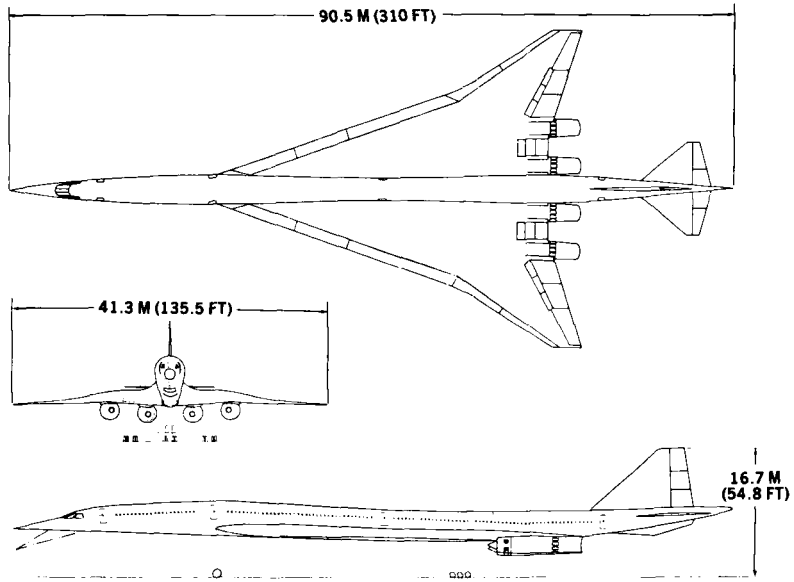
PLANFORM REFERENCE NUMBER	DATA USING BASELINE* AIRCRAFT SKIN FRICTION AND WAVE DRAG			COMPLETE AIRCRAFT L/D
	GROSS WING L/D	WING/BODY L/D	WING BODY, TRIMMED L/D	
W33	9.75	9.91	10.10	9.75
W34*	8.69	8.76	9.10	9.10
W35	9.09	9.25	9.64	9.60
W36	8.32	8.39	8.66	
W37	8.61			
W38	10.50**			
W39	9.64	9.60	9.80	9.75
W40	9.18**			

*BASELINE

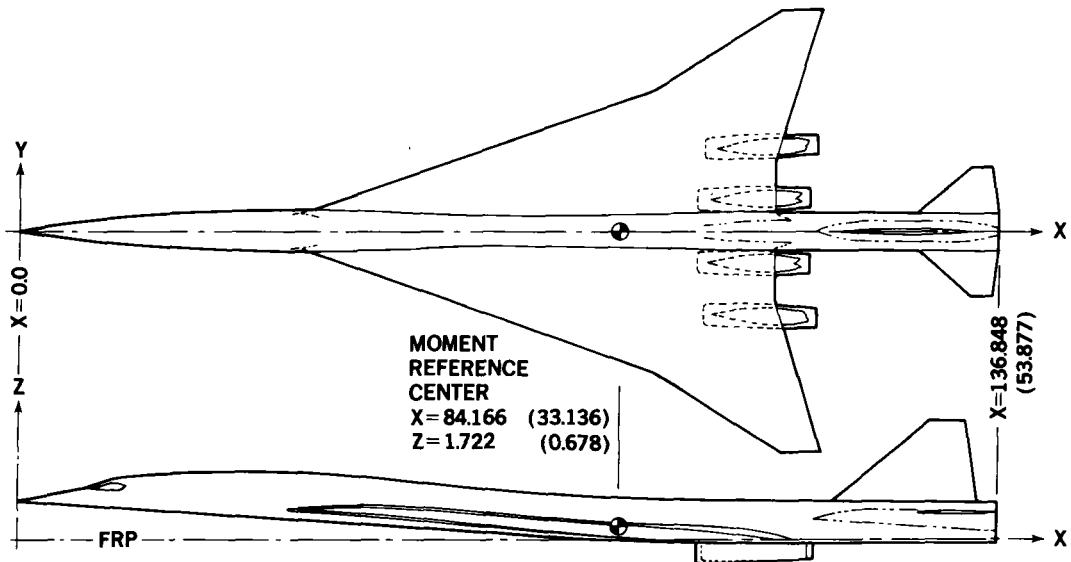
**DROPPED DUE TO STRUCTURAL LIMITATIONS

TABLE 3.- WING PLANFORMS FOR ASPECT RATIO STUDY

PLANFORM REFERENCE NUMBER	ASPECT RATIO	LEADING EDGE			TRAILING EDGE
		∧ INBOARD (DEGREES)	LEADING EDGE BREAK (%SEMISPAN)	∧ OUTBOARD (DEGREES)	∧ OUTBOARD (DEGREES)
W35	1.84	71	70	61.5	31
W41	2.08	71	70	62	40
W42	2.08	67	70	62	30
W44	1.70	72	70	62	30
W45	2.09	71	65	61.5	31
W47	1.61	71	75	61.5	31



(a) Configuration details.



(b) High-speed wind tunnel model details.

Figure 1.- McDonnell Douglas D3230-2.2-5 configuration and model details.

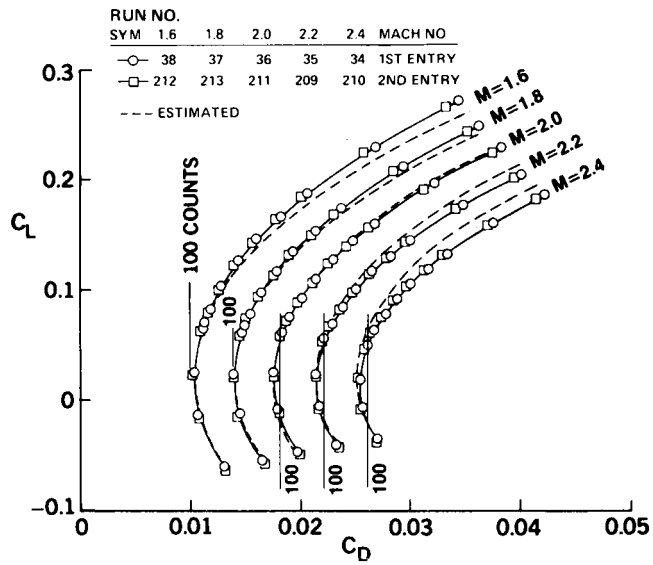


Figure 2.- Comparison of estimated and experimental drag polars for B_1W_2 , Mach 1.6 to 2.4.

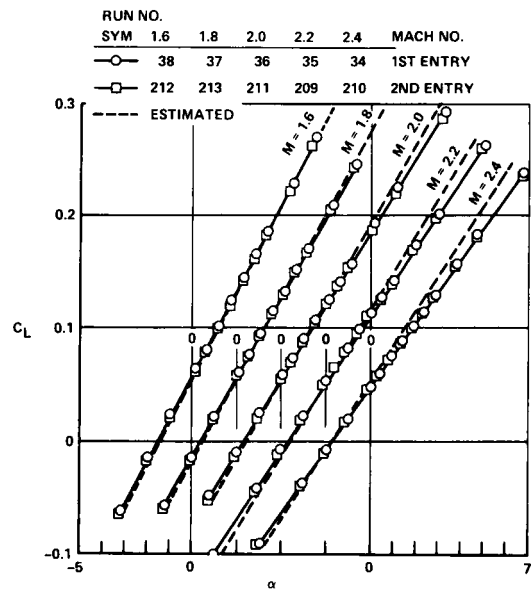


Figure 3.- Comparison of estimated and experimental lift curves for B_1W_2 , Mach 1.6 to 2.4.

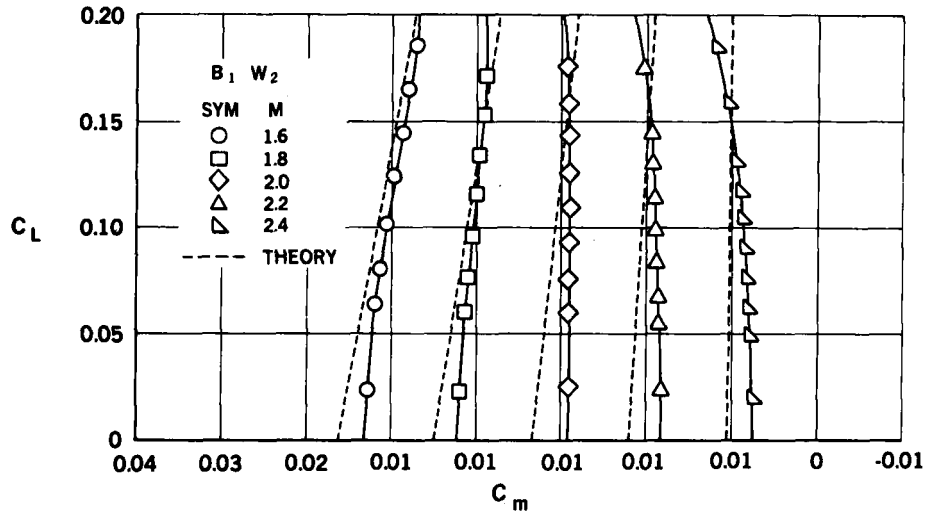


Figure 4.- Experimental and estimated supersonic pitching moments for $B_1 W_2$.

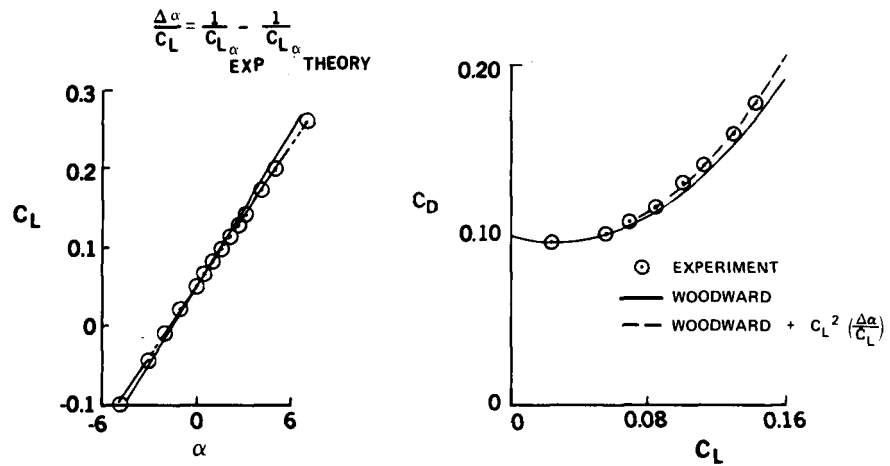


Figure 5.- Derivation of the transonic leading edge correction; 2.2 M.

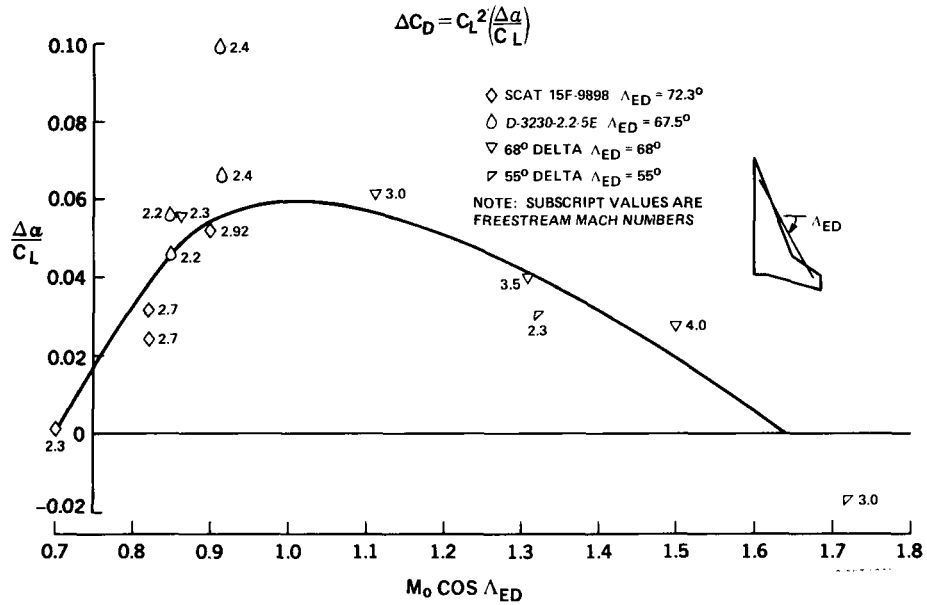


Figure 6.- Transonic leading edge (TLE) correction. (Semi-empirical correction of Woodward for improved drag prediction.)

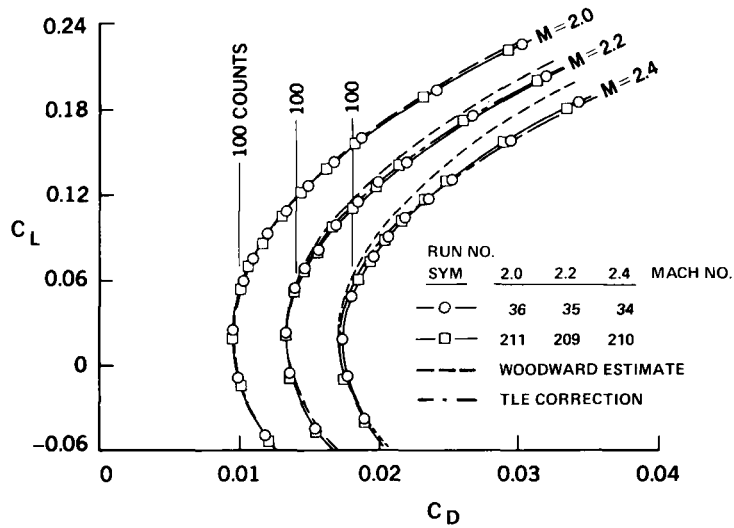


Figure 7.- Effect of TLE correction on estimated drag polars for B₁W₂, Mach 2.0 to 2.4.

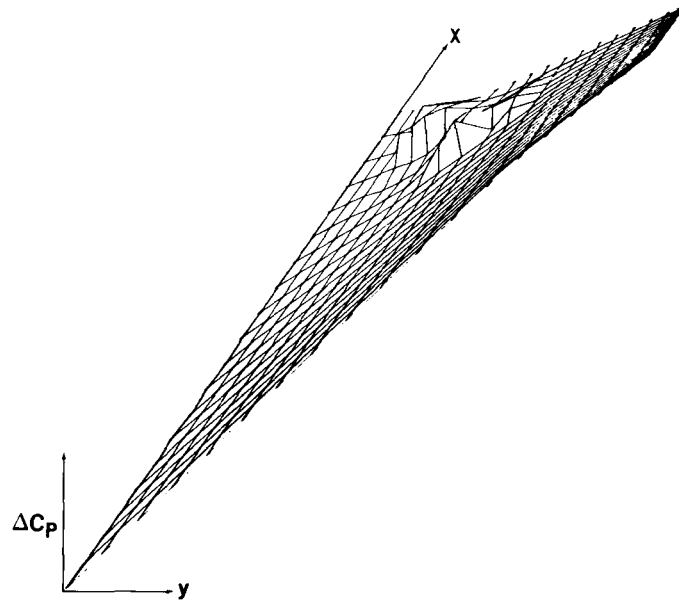


Figure 8.- Pictorial representation of nacelle-on-wing interference pressures.

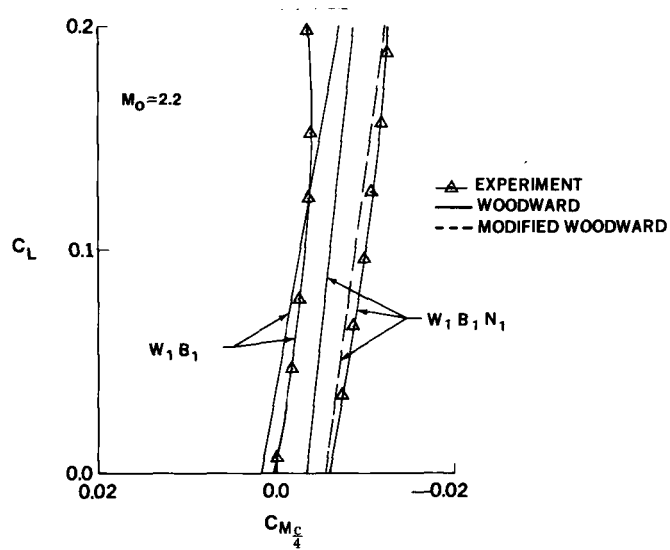


Figure 9.- Comparison of Woodward with nacelle interference modifications and experimental pitching moments; tail off, 2.2 M.

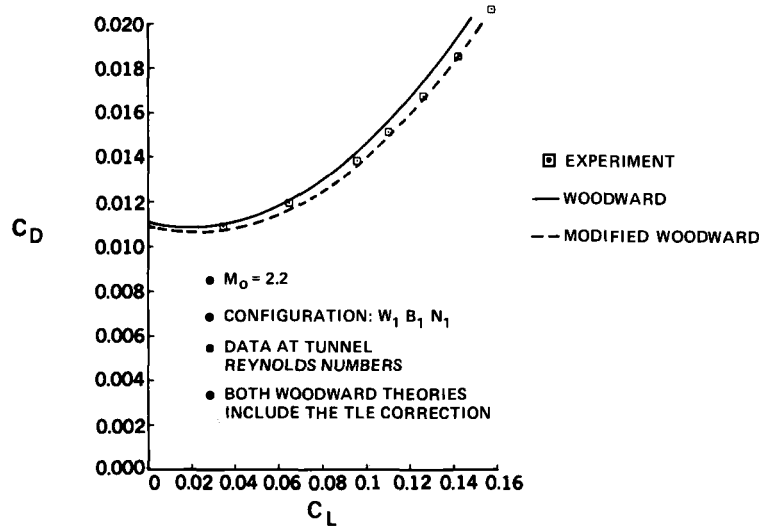


Figure 10.- Comparison of Woodward with nacelle interference modifications and experimental drag polars; 2.2 M.

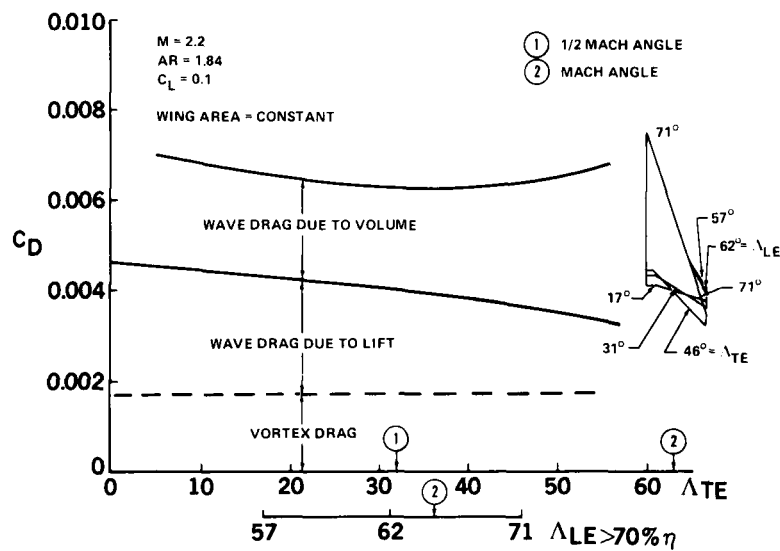


Figure 11.- Effect of trailing-edge sweep on induced drag and wave drag.

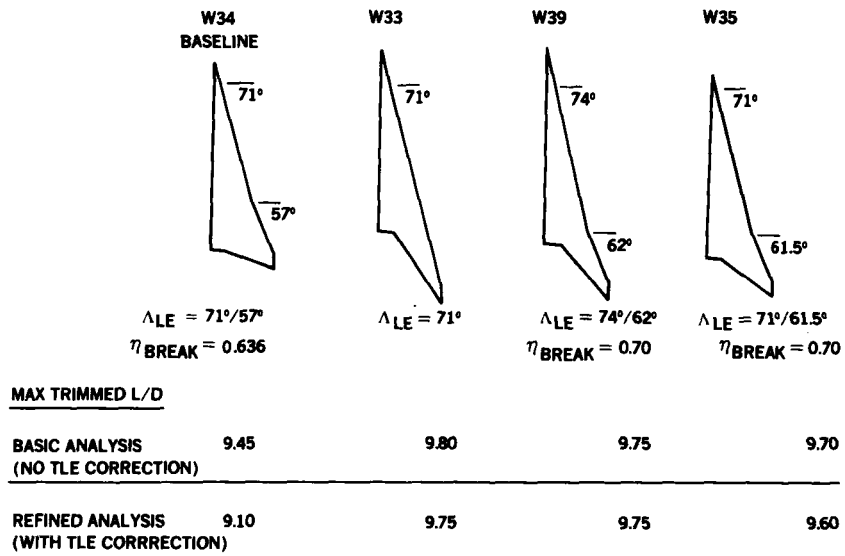


Figure 12.- Wing planform study, summary of selected wings; 2.2 M.

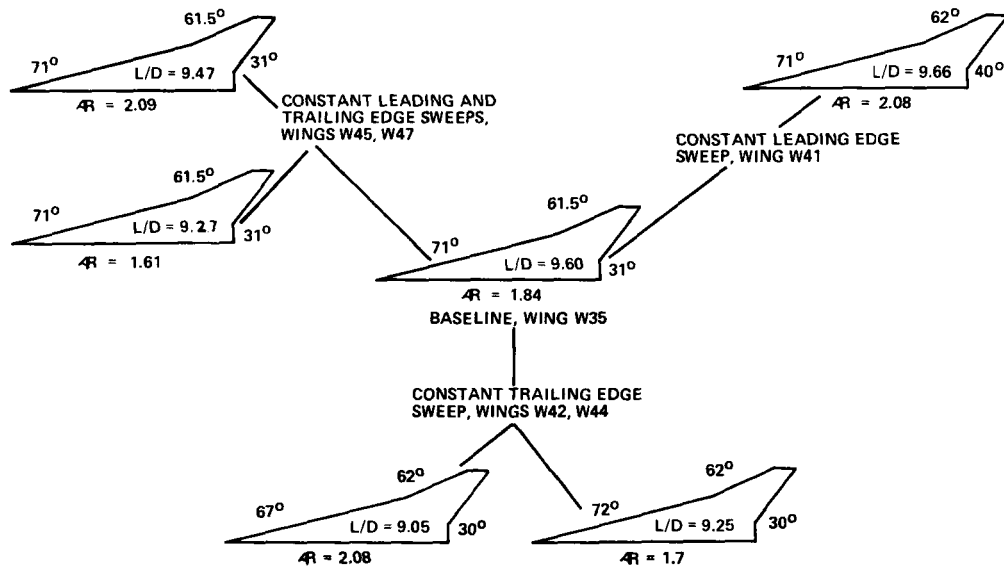


Figure 13.- L/D variations with aspect ratio; 2.2 M.

DEFINITION OF REFLEX ANGLE

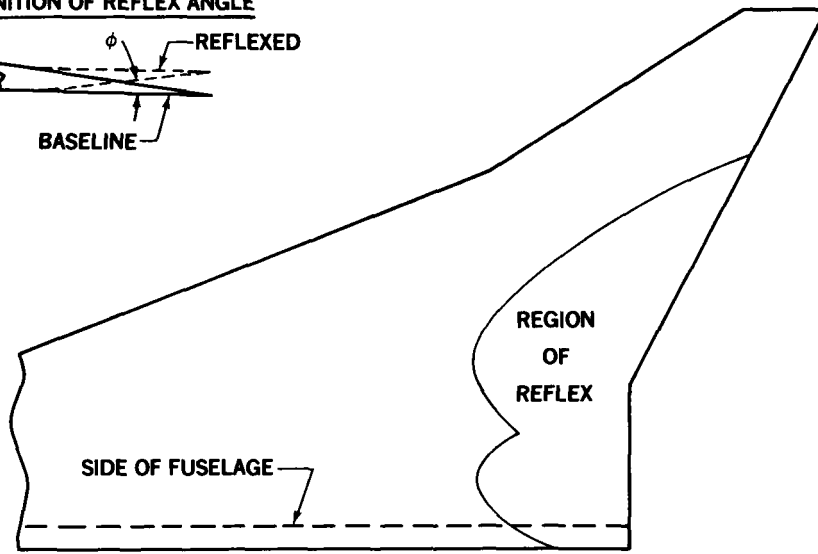
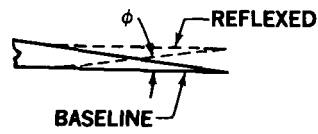


Figure 14.- Reflex in region of nacelle interference.

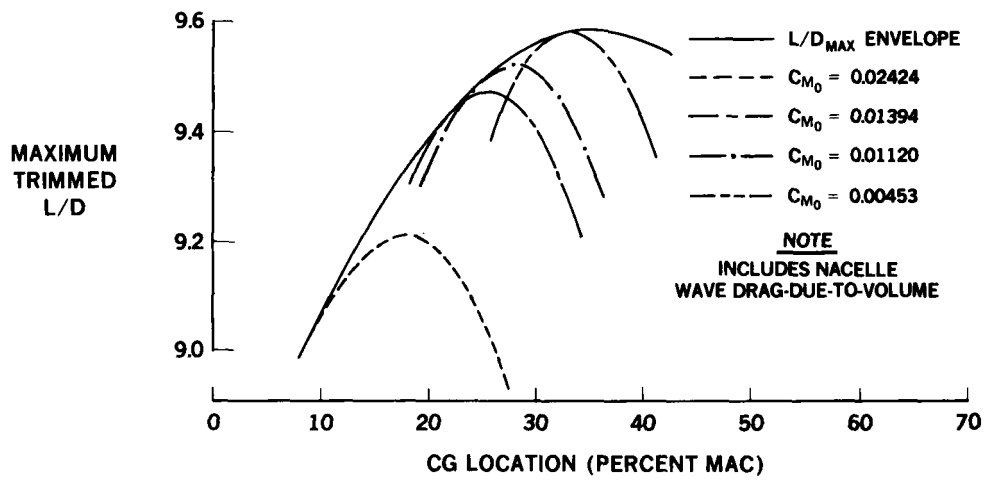


Figure 15.- Selection of wing pitching moment for optimum trimmed L/D; 2.2 M, nacelles off.

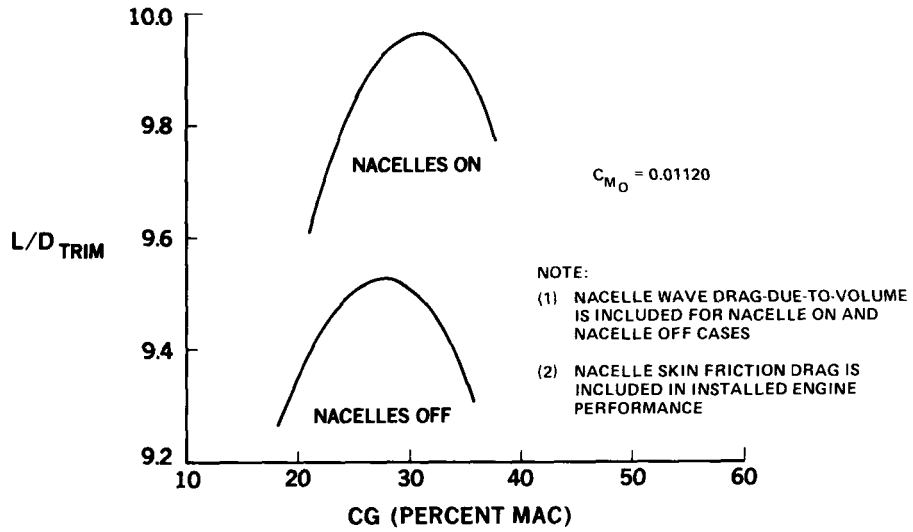


Figure 16.- Effect of nacelle addition on a pitch constrained wing; 2.2 M.

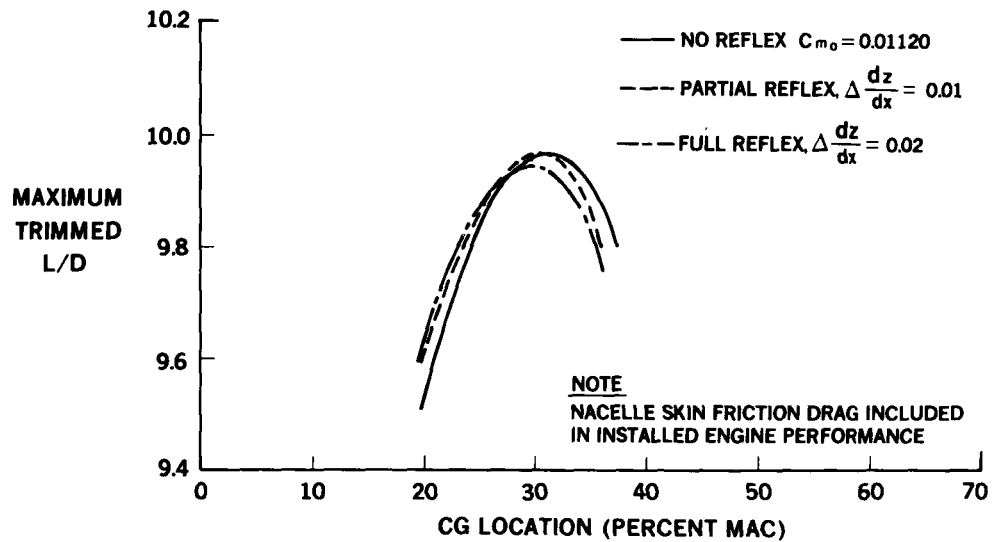


Figure 17.- Effect of reflex for nacelles on a pitch constrained wing; 2.2 M, nacelles on.

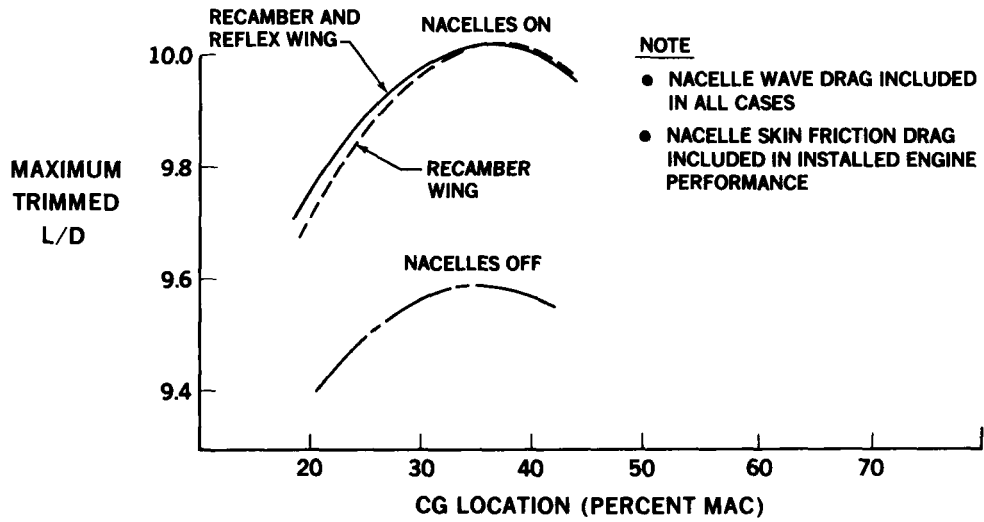


Figure 18.- Design L/D envelopes for nacelle addition with wing reflex and recamber; 2.2 M.

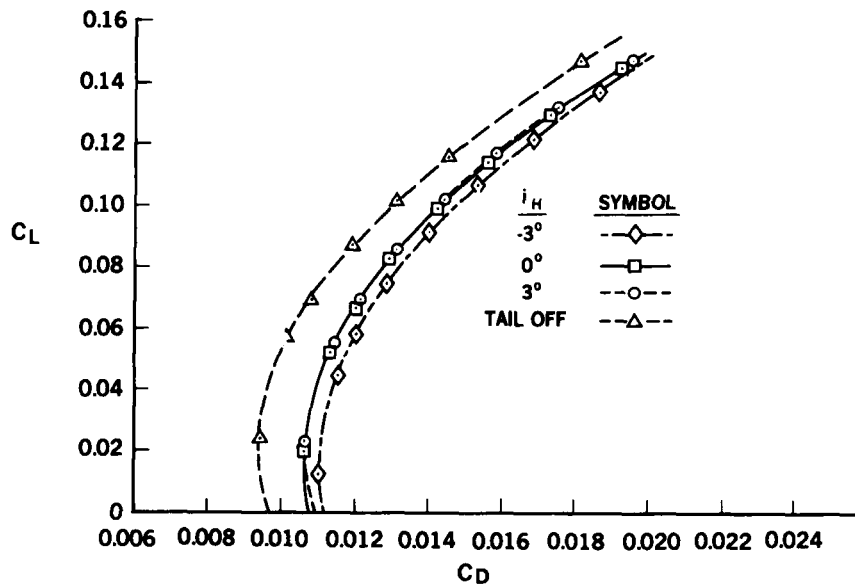


Figure 19.- Experimental tail on and off drag polars; 2.2 M.

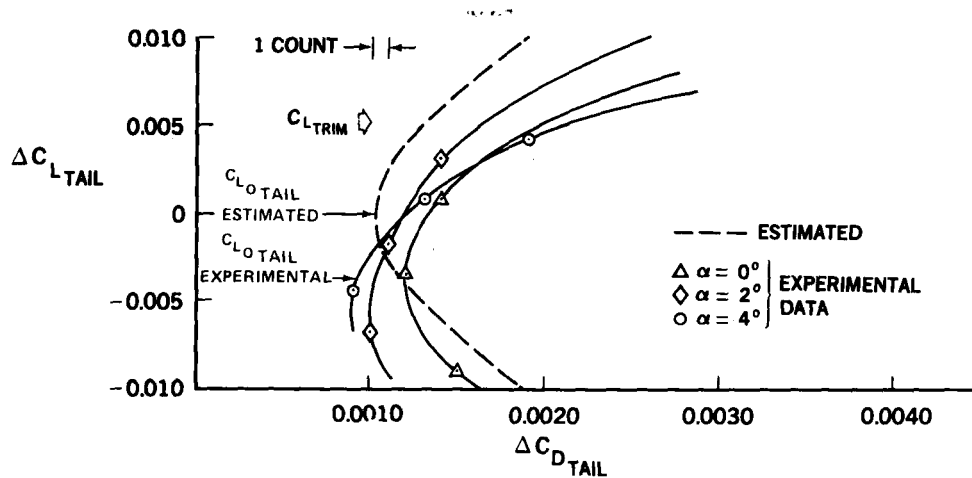


Figure 20.- Horizontal tail drag polars; 2.2 M, coefficients based on wing area.

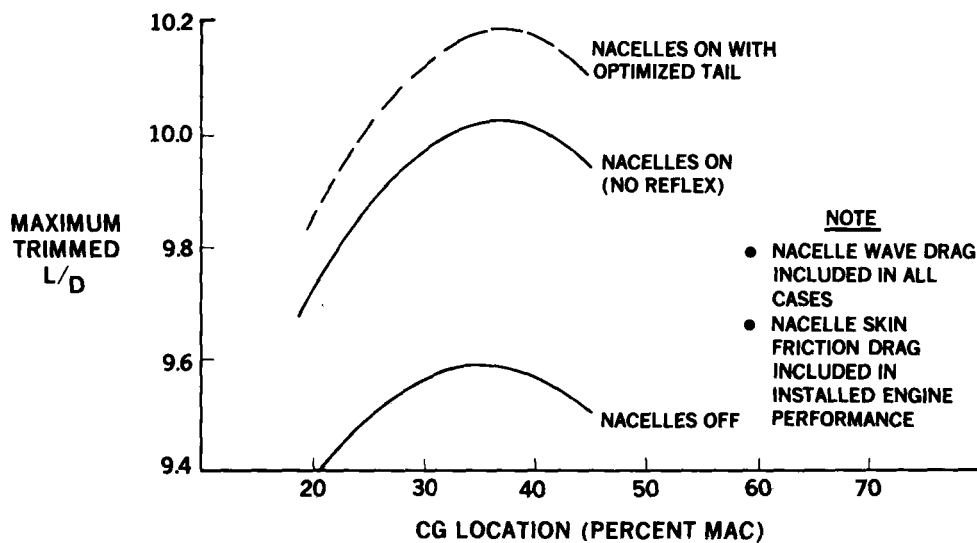


Figure 21.- Effect of optimized tail on design L/D envelopes; 2.2 M.

- TLE CORRECTION USED TO IMPROVE WOODWARD ESTIMATES
- WING W35 SELECTED AS NEW PLANFORM
- MODIFIED WOODWARD PROGRAM ACCURATELY PREDICTS EFFECT OF NACELLES
- WING RECAMBER PRODUCES FAVORABLE NACELLE INTERFERENCE
- WING REFLEX NOT NEEDED IF CG CAN BE ALLOWED TO VARY
- HORIZONTAL TAIL SHOULD BE OPTIMIZED FOR ITS TRIM LIFT
- IMPROVED METHODS ARE REQUIRED TO PROPERLY DESIGN AN OPTIMIZED TAIL

Figure 22.- Conclusions.

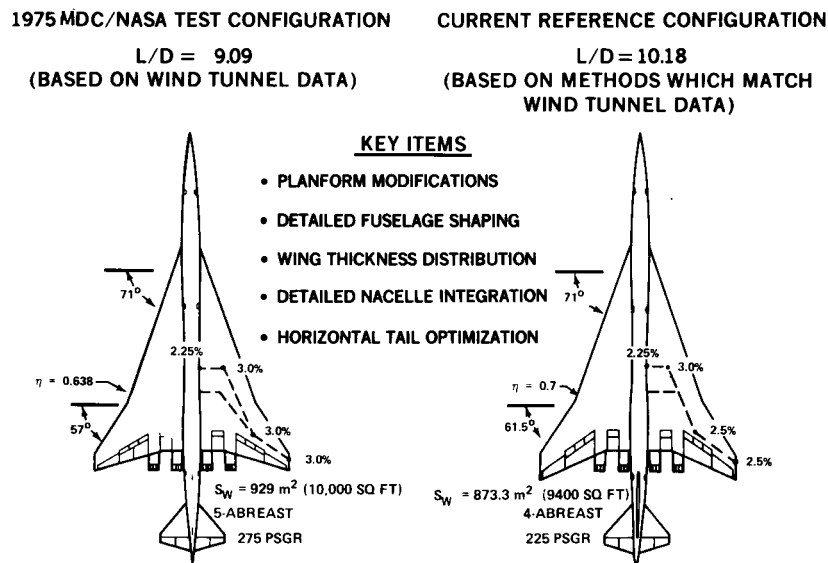


Figure 23.- Refined aerodynamic configuration; MDC/NASA test configuration compared with current reference configuration.

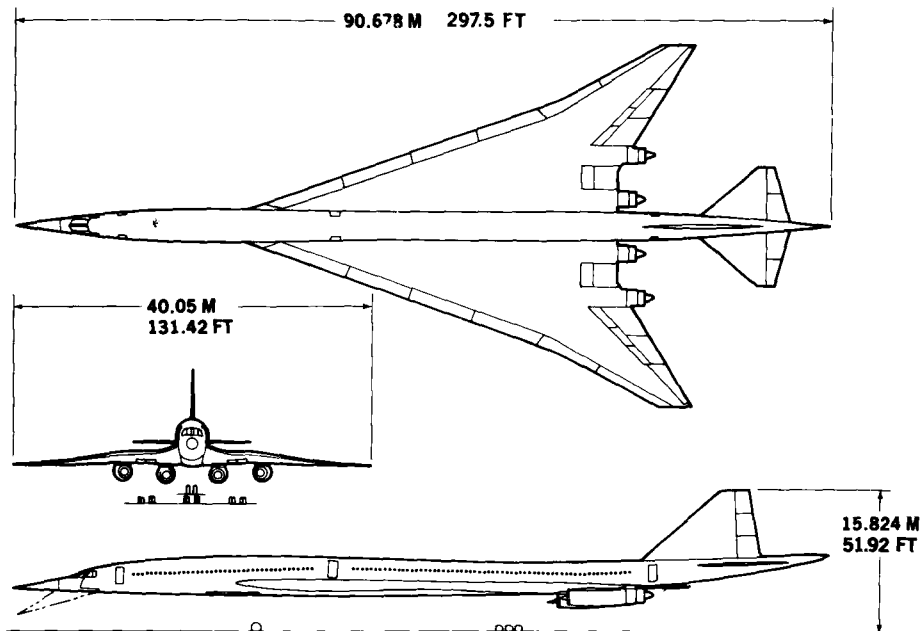


Figure 24.- Details of McDonnell Douglas D3232-2.2-3 configuration.